Revista Mexicana de Astronomía y Astrofísica, **52**, 347–355 (2016)

VARIABILITY OF THE EMISSION LINE FLUXES AND RATIOS OF HH 1/2

A. C. Raga,[1] B. Reipurth,[2] A. Castellanos-Ramírez,[1] and J. Bally[3]

Received April 18 2016; accepted June 7 2016

RESUMEN

Comparamos datos espectrofotométricos obtenidos en 1978 (por Brugel et al. 1981a) con los flujos de líneas de emisión de imágenes calibradas obtenidas con el Hubble Space Telescope (HST) en 1994 y 2014. Esta comparación muestra que los cocientes de líneas de emisión de estos objetos se han mantenido sorprendentemente invariantes durante los últimos 36 años. Por otro lado, las intensidades de las líneas sí han cambiado, y muestran un incremento por un factor de ≈ 4 para HH 2, y un decremento de $\approx 30\%$ para HH 1. Estos resultados apoyan la idea de que HH 1 y 2 son cabezas de jets densos, viajando en un medio ambiente con densidad decreciente (para HH 1) o creciente (para HH 2).

ABSTRACT

We compare spectrophotometric data of HH 1 and 2 obtained in 1978 (by Brugel et al. 1981a) with the emission line fluxes from calibrated Hubble Space Telescope (HST) images obtained in 1994 and 2014. This comparison shows that the emission line ratios of these objects have remained surprisingly invariant during the past 36 years. On the other hand, the line intensities have indeed changed, with HH 2 brightening by a factor of ≈ 4 and HH 1 becoming $\approx 30\%$ fainter. These results would be consistent with HH 1 and 2 being leading working surfaces of heavy jets travelling into an environment of decreasing (for HH 1) or increasing (HH 2) densities.

Key Words: Herbig-Haro objects — ISM: individual objects (HH1/2) — ISM: jets and outflows — shock waves — stars: formation — stars: winds, outflows

1. INTRODUCTION

Even though it is clear that the Herbig-Haro objects HH 1 and 2 have strong time-variabilites (Herbig 1969, 1973; Herbig & Jones 1981; Brugel et al. 1985; Raga et al. 1990a; Böhm et al. 1993; Eislöffel et al. 1994), the study of their time-dependent emission spectrum has proven to be quite difficult. The difficulties arise from the heterogeneity of the data.

The older images of HH 1 and 2 (before ≈ 1985) are relatively broad band photographic plates, and have been analyzed by Herbig (1969, 1973) for time variabilities. The analysis presented in these papers to some extent stands alone, since it is not straightforward to relate it to more recent observations (obtained with different techniques).

More recent CCD images of HH 1 and 2 obtained through narrow-band filters, cover very few emission lines, and in general lack any calibration. As far as we are aware, the only attempts to use ground based CCD images for an evaluation of the variability of HH 1 and 2 were presented by Raga et al. (1990a) and by Eislöffel et al. (1993).

Spectrophotometric observations of HH 1 and 2 have generally been obtained either with "short" (Hartigan et al. 1987) or "long" (Solf et al. 1988; Giannini et al. 2015) spectrograph slits. Though the obtained spectra are generally well calibrated, it is difficult to disentangle the time-variability of the angularly extended HH 1 and 2 objects from effects due to different slit sizes and positions of the successive

[1]Instituto de Ciencias Nucleares, Universidad Nacional Autónoma de México, Ciudad de México, México.
[2]Institute for Astronomy, Univ. of Hawaii at Manao, Hilo, USA.
[3]Center for Astrophysics and Space Astronomy, Univ. of Colorado, Colorado, USA.

observations. Also, spectrophotometric observations of Brugel et al. (1981a, b) are available, which cover at least most of the emitting regions of HH 1 and 2 (see below and § 2).

The HH 1 and 2 images obtained with the Hubble Space Telescope (Hester et al. 1998; Bally et al. 2002; Hartigan et al. 2011; Raga et al. 2015a, b; Raga et al. 2016) have calibrated fluxes, and are therefore appropriate for studying the time-dependence of the emission. An analysis of the time-variability of the [O III] 5007, Hα and [S II] 6716+30 emission of HH 1 in this images was presented by Raga et al. (2016). Also, a "pre-COSTAR" set of HST images of HH 2 (in Hα, [S II] and [O III]) was obtained by Schwartz et al. (1993).

In Figure 1 we present a comparison between a photograph of HH 2 obtained by Herbig in 1959 (in red light, with the Lick Observatory 120-inch reflector shortly after its inauguration), and the addition of an Hα and a [S II] 6716+30 frame obtained with the Hubble Space Telescope in 2014 (see Raga et al. 2015a, b). The two images have been scaled and centered in an approximate way. From this figure, it is clear that the structure of HH 2 has changed in a dramatic way over the past ≈ 55 years.

In the present paper, we use the two sets of HST images which cover a broader range of emission lines, namely,

- the 1994 images of Hester et al. (1998), which include filters isolating the [O III] 5007, Hα and [S II] 6716+30 lines,
- the 2014 observations of Raga et al. (2015a,b) which include the Mg II 2798 (not described in the published papers), [O II] 3726+28, Hβ, [O III] 5007, [O I] 6300, Hα and [S II] 6716+30 lines.

The second (2014) set of HST images covers most of the bright near-UV to optical emission lines of HH 1 and 2, and is therefore appropriate for studying the time-evolution of the spectra of these objects. Unfortunately, the first (1994) set has only three images, and can only be used for an analysis of the time-evolution of the three line combinations.

For an analysis of more emission lines, we can use the spectrophotometric observations of Brugel et al. (1981a). These authors used a multi-channel spectrophotometer with apertures that covered most of the emitting regions of HH 1 and 2. These observations can be directly compared with line fluxes calculated by angularly integrating the 1994 and 2014 sets of HST images over the emitting areas of HH 1 and HH 2.

In this way, we use the immensely detailed HST images only for obtaining an angularly integrated emission line spectrum of HH 1 and 2, and we compare the resulting spectra with the spectrophotometric observations of Brugel et al. (1981a). We feel that the somewhat brutal angular integration of the HST images is justified by the very interesting comparison that can be made with the older spectrophotometric results.

The paper is organized as follows. The HST images and the older, spectrophotometric data sets are discussed in § 2. The 2014 Mg II 2798 HST image (which has not been presented before in the literature) is also presented in this section. § 3 presents an evaluation of the time-evolution of the emission line spectra of HH 1 and 2. § 4 discusses a simple working surface model which is used for interpreting the observed time-dependence of the line emission. Finally, the results are discussed in § 6.

2. THE OBSERVATIONS

2.1. *The reddening correction*

Brugel et al. (1981a) used Miller's (1968) method, which is based on the fixed ratio of the transauroral (4069, 4076Å) to the auroral (10318, 10336Å) [S II] lines, and obtained $E(B-V) = 0.47$ for HH 1 and $E(B-V) = 0.35$ for HH 2. Raga et al. (2015b) used the average of the Hα/Hβ ratios of the individual emitting pixels of HH 1 and 2 to derive $E(B-V) \approx 0.27$ for the two objects.

In this paper, we present the observed line fluxes and ratios, as well as the values corrected for a standard Galactic extinction curve with $E(B-V) = 0.27$. This extinction curve (see Fitzpatrick 1999) corresponds to the $R = A_V/E(B-V) = 3.1$ case of Cardelli et al. (1988). This choice is not unique, since there has been a considerable amount of discussion as to which extinction curve is actually relevant for the HH 1/2 region (see, e.g., Böhm-Vitense et al. 1982 and Böhm et al. 1991). The choice of extinction curve of course has a particularly strong effect in the UV.

2.2. *The first epoch spectrophotometric observations*

In September 1978, Brugel et al. (1981a) observed HH 1 and 2 with the MCSP II spectrophotometer (see Oke 1969) at the Palomar 5.1 m telescope. In the configuration that was used the spectrophotometer had an aperture of 6″ diameter (see Brugel et al. 1981b), and several positions (2 for HH 1 and 3 for HH 2) were used to cover the emitting regions of HH 1 and 2. We have now co-added

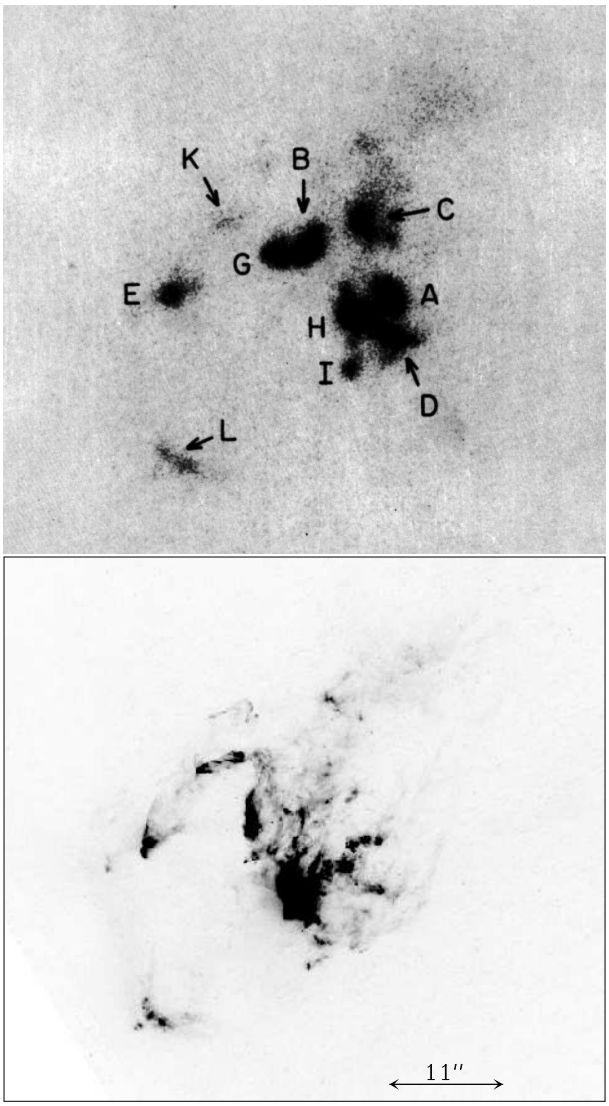

Fig. 1. Comparison between a photograph of HH 2 (obtained by G. Herbig in 1959 at the Lick Observatory 120-inch reflector, top) and an Hα+[S II] image (obtained in 2014 with the HST, shown with a linear greyscale). The two images have been approximately scaled and centered relative to each other. The identifications of the condensations of HH 2 are given in the top frame, and the angular scale is shown in the bottom frame. N is up and E to the left.

the spectra from the two HH 1 apertures and the three HH 2 apertures to obtain two spectra: one for HH 1 and one for HH 2.

These spectra include the [O II] 3726+28, Hβ, [O III] 5007, [O I] 6300 and Hα lines. Unfortunately, the channels of the MCSP cover the [S II] 6716 but not the [S II] 6730 line. Because of this, we have taken the [S II] 6716+6730/Hα ratio from a lower quality spectrum obtained by Brugel et al. (1981a) at the KPNO 2.1 m telescope.

Finally, for the Mg II 2798 line we have taken the fluxes obtained in 1980 with the International Ultraviolet Explorer (IUE) by Böhm-Vitense et al. (1982). The IUE spectrograph had a $23'' \times 10''$ aperture, which included most of the emitting regions of HH 1 and 2. As this UV observation was carried out only a couple of years after the Brugel et al. (1981a) optical observations. In the following we consider them as taken at the same time.

2.3. *The HST images*

We consider two epochs of HST images:

1. the [S II] 6716+30, Hα and [O III] 5007 images of Hester et al. (1998), obtained in 1994.6,

2. the [S II] 6716+30, Hα, [O I] 6300, [O III] 5007, Hβ, and [O II] 3726+28 images of Raga et al. (2015a), obtained in 2014.6.

To the 2014.6 set of images, we have added a Mg II 2798 image (a 5484 s exposure through the F280N filter) which was not analyzed by Raga et al. (2015a). Figure 2 shows the brighter region of HH 2 in the Hα, Hβ, and Mg II 2798 dereddened images, and the Mg II/Hβ line ratio map. HH 1 is barely visible in the Mg II 2798 frame, but an angularly integrated flux for HH 1 can be obtained.

There are two other epochs of HST images of HH 1 and 2 (see Bally et al. 2002 and Hartigan et al. 2011), but we do not include them in the present study because they only cover the [S II] 6716+30 and Hα lines.

As discussed by Raga et al. (2015a), the continuum emission of HH 1 and 2 affects the line fluxes obtained from the HST images. This continuum contamination is more important for the blue lines, and it could be as large as $\approx 30\%$ for the Mg II 2798 line. However, this is unlikely to have a large effect for the qualitative interpretation of the emission proposed in the present paper.

In order to compare the HST line fluxes with the spectrophotometric data of Brugel et al. (1981a), we carry out angular integrations over the emitting areas of HH 1 and 2 in the HST frames. In order to do this, we add the emission within the 5×10^{-15} erg s^{-1}cm^{-2}arcsec^{-2} (dereddened) Hα isophotes of HH 1 and 2. In this way, we avoid defining arbitrary "boxes" around both objects.

2.4. *The Mg II 2798 image*

Figure 2 shows the Mg II 2798 HST image obtained in 2014 (see subsection 2.3). We see that the Mg II emission has an angular extent comparable to that of the Hβ emission (fainter, more extended regions being seen in Hα). Because of this, we have chosen to calculate the Mg II/Hβ ratio map (which depends much less on the reddening correction than the Mg II/Hα ratio), which is also shown in Figure 2. We do not display the Mg II emission of HH 1 because it is quite faint, so that it is only appropriate for obtaining an angularly integrated line flux.

From the line ratio map, we see that most of the Mg II emitting region of HH 2 (within condensation H) has a Mg II/Hβ ratio of $\approx 1 \rightarrow 2$. If one looks at the predictions from the plane-parallel shock models of Hartigan et al. (1987), one sees that these line ratios are consistent with shock velocities between 110 and 160 km s^{-1}.

There is also a small region in the NE of condensation H with Mg II/H$\beta \approx 5$, implying a shock velocity of ≈ 260 km s^{-1} (see Hartigan et al. 1987).

3. THE TIME-DEPENDENT LINE RATIOS AND FLUXES

In Table 1, we present the observed and dereddened Hα fluxes obtained in the three epochs of observations described in § 2. This table gives the measured (F) as well as the dereddened (F_0) fluxes, which were obtained assuming a standard Galactic extinction curve with $E(B-V) = 0.27$ (for both HH 1 and 2, see § 2.1). We have also computed the Hα luminosities with the dereddened fluxes and a distance of 414 pc to HH 1 and 2.

It is clear that the Hα luminosity of HH 1 has a slowly decreasing trend, with a decrease of $\approx 4\%$ from 1978.7 to 1994.6 and a somewhat larger decrease of $\approx 24\%$ from 1994.6 to 2014.6. On the other hand, HH 2 has an Hα luminosity which increases by a factor of ≈ 2.4 from 1978.7 to 1994.6 and by a factor of ≈ 1.75 from 1994.6 to 2014.6.

In Table 2, we present the observed and dereddened line ratios of HH 1 and 2. For both objects, the spectrum has a surprisingly small time-dependence. For HH 1:

- the Mg II 2798 line (relative to Hα) has not changed appreciably from 1980.7 to 2014.6. Unless we have a strange coincidence, this result seems to imply both that the variations of the intrinsic spectrum are small and that the extinction to HH 1 has remained invariant during this time-period,
- the [O II] 3726+29 lines have grown by $\approx 40\%$ from 1978.7 to 2014.6,
- the Hβ line has a relatively low value compared to Hα in the 1978.7 spectrum. This might be an indication that the regions of HH 1 with collisionally excited lines could have contributed more to the spectrum of HH 1 than in 2014.6 (when the regions of high Hα/Hβ ratio have small angular extents, see Raga et al. 2015b),
- the [O III] 5007 line grew by a factor of 2 from 1978.7 to 1994.6, and then decreased by $\approx 20\%$ in the 2014.6 observations,
- the [O I] 6300 line has had a small increase from 1978.7 to 2014.6,
- the [S II] 6716+30 lines have grown (relative to Hα) by a factor of ≈ 2 from 1978.7 to 2014.6.

For HH 2:

- the Mg II 2798 line has grown by a factor of 2 from 1980.7 to 2014.6. This could be due to the fact that the aperture of the IUE spectrograph (used for the 1980.7 observations see § 2) might not have included all of the emitting region of HH 2. Also, the continuum contamination in the HST image could be responsible for part of this increased flux (however, a corresponding increase should then be seen in HH 1),
- the [O II] 3726+29 lines have grown (relative to Hα) by $\approx 20\%$ from 1978.7 to 2014.6,
- the [O III] 5007 line grows by $\approx 40\%$ from 1978.7 to 1994.6, and in 2014.6 returns to a value very similar to the 1978.7 value,
- the Hβ, [O I] 6300 and [S II] 6716+30 lines have very small variations (relative to Hα).

4. INTERPRETATION IN TERMS OF A WORKING SURFACE MODEL

4.1. *General considerations*

The variations in the emission line ratios for HH 1 are not large, but might be significant (in particular, for the [S II] and [O II] lines). The spectrum of HH 2 shows smaller line ratio variations, except for the Mg II 2798 line (an effect which might be due to part of the emitting region falling outside the IUE spectrograph aperture of the 1980.7 observations). Therefore, we conclude that the emission line spectra of HH 1 and 2 have at most shown small variabilities in their *relative* line intensities (see Table 2).

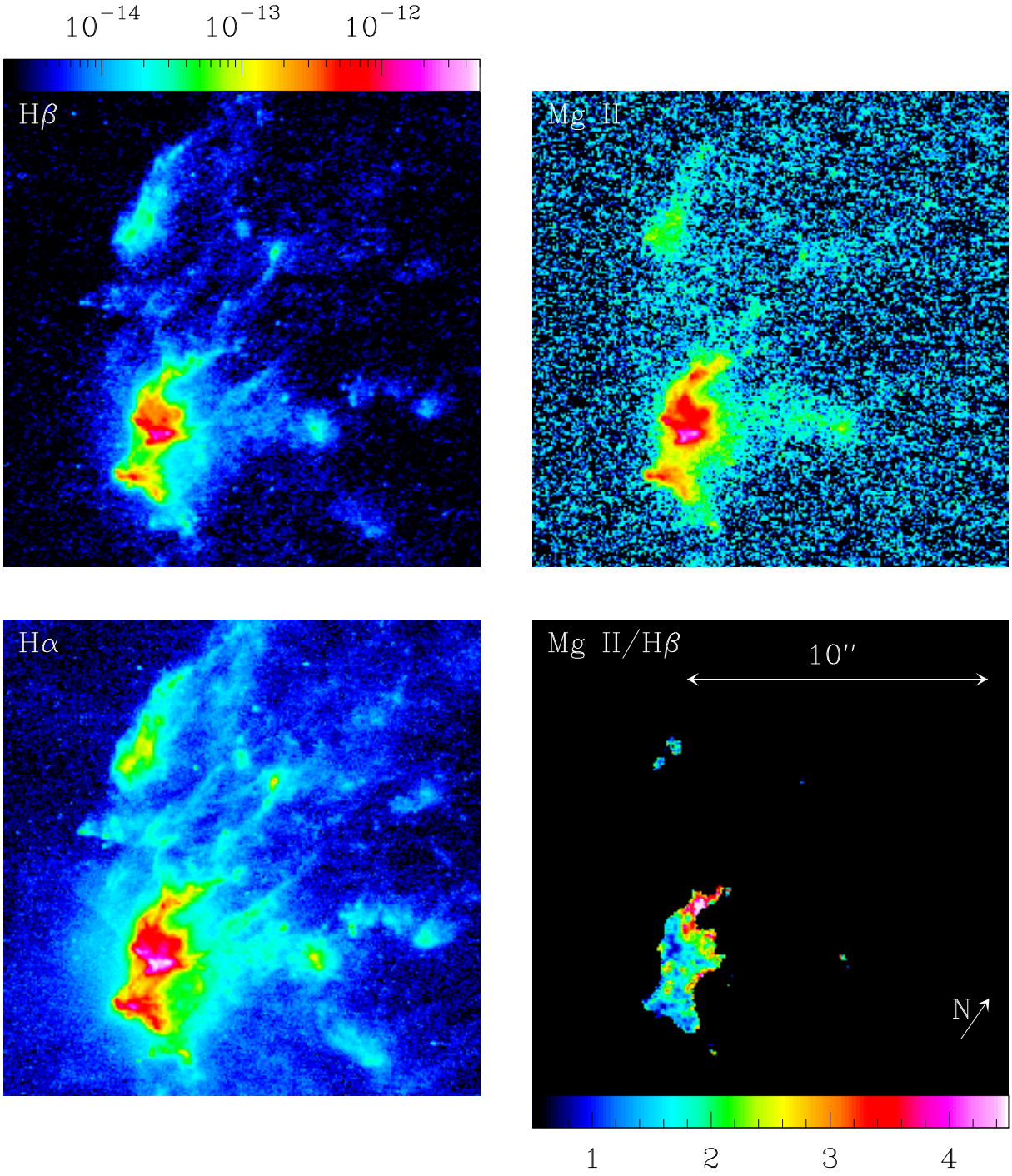

Fig. 2. Hβ (top left), Hα (bottom left), Mg II 2798 (top right) and Mg II/Hβ line ratio (bottom right) maps of HH 2. The emission maps are shown with the logarithmic color scale (in erg s^{-1} cm^{-2} $arcsec^{-2}$) displayed in the top left bar. The line ratio map is shown with the linear color scale displayed in the bottom right bar. The angular scale and orientation of the frames are shown in the bottom right frame. The color figure can be viewed online.

TABLE 1

Hα LINE FLUXES AND LUMINOSITIES

Epoch	HH 1			HH 2		
	$F_{H\alpha}$[1]	$F_{H\alpha,0}$[1]	$L_{H\alpha}$[2]	$F_{H\alpha}$[1]	$F_{H\alpha,0}$[1]	$L_{H\alpha}$[2]
2014.6	4.16	7.50	4.05×10^{-3}	33.67	60.75	3.28×10^{-2}
1994.6	5.50	9.92	5.36×10^{-3}	19.21	34.67	1.87×10^{-2}
1978.7	5.77	10.41	5.63×10^{-3}	7.88	14.21	7.68×10^{-3}

[1]Observed (F) and dereddened (F_0) Hα fluxes in units of 10^{-13} erg s^{-1} cm^{-2}.

[2]Luminosities (in units of $L_\odot$) assuming a distance of 414 pc.

HH 1 shows a small decrease in Hα flux of ≈ 30% from 1978 to 2014. On the other hand, the Hα flux of HH 2 shows a clear, monotonic increase as a function of time.

Unless we have a combination of effects cancelling each other out, we can conclude that the invariance of the line ratios implies that:

- a time-independent interstellar extinction correction (such as the one which we have applied, see § 2) appears to be appropriate,
- the shock velocities associated with HH 1 and 2 do not change substantially as a function of time.

As can be seen from steady, plane-parallel shock models (see, e.g., Raymond 1979 and Hartigan et al. 1987), the emission line ratios of the spectrum emitted by a shock are generally a strong function of shock velocity, and only depend weakly on the preshock density. Also, shocks (of a given shock velocity) with a cooling function dominated by processes in the "low density regime" have line fluxes that scale linearly with the preshock density.

Therefore, an increase in the emission line flux (and at the same time keeping approximately constant line ratios) such as is seen in HH 2 implies that the emission is produced in shocks with approximately time-independent shock velocities, and with a pre-shock density that increases with time. How can this situation be obtained in a working surface of a jet? This question is addressed in the following section.

4.2. *The luminosity of a working surface*

A working surface is composed of a "jet shock" that slows down the jet material (on interaction with the environmental gas) and a "bow shock" which accelerates ambient material. From the standard, ram-pressure balance argument, for the two-shock working surface one obtains a velocity of motion (Raga et al. 1990b):

$$v_{ws} = \frac{\beta(1+\alpha)}{1+\beta} v_j \,, \tag{1}$$

where v_j is the jet velocity, $\beta = \sqrt{\rho_j/\rho_a}$ (where ρ_j and ρ_a are the jet and ambient densities, respectively) and $\alpha = v_a/v_j$ (where v_a is a possibly non-zero velocity away from the source of the ambient medium into which the jet is propagating). Equation (1) applies for the leading head of the jet (by setting $\alpha = 0$) or to an "internal working surface" within a variable jet (see Raga et al. 1990b), moving into previously ejected, slower jet material.

The jet shock has a shock velocity:

$$v_{js} = v_j - v_{ws} = \frac{1-\alpha}{1+\beta} v_j \,, \tag{2}$$

and the shock velocity of the bow shock is:

$$v_{bs} = v_{ws} - v_a = \frac{\beta(1-\alpha)}{1+\beta} v_j \,. \tag{3}$$

Now, in a highly radiative shock most of the kinetic energy flux arriving at the shock ends up being radiated away. Therefore, assuming that the jet and bow shocks have approximately the same surface area σ, the luminosities of the jet shock and the bow shock are:

$$L_{js} = \frac{\sigma \rho_j v_{js}^3}{2} = \frac{\dot{M}_j}{2} \left(\frac{1-\alpha}{1+\beta}\right)^3 v_j^2$$

$$= \frac{\dot{M}_j}{2} \frac{(1-\alpha)^3 v_{ws}^2}{\beta^2 (1+\beta)(1+\alpha)^2} \,, \tag{4}$$

$$L_{bs} = \frac{\sigma \rho_a v_{bs}^3}{2} = \frac{\dot{M}_j}{2} \left(\frac{1-\alpha}{1+\beta}\right)^3 \beta v_j^2$$

$$= \frac{\dot{M}_j}{2} \frac{(1-\alpha)^3 v_{ws}^2}{\beta (1+\beta)(1+\alpha)^2} \,, \tag{5}$$

TABLE 2

EMISSION LINES WITH RESPECT TO Hα = 100

Ion	λ [Å]	Epoch	HH 1		HH 2	
			F	F_0	F	F_0
Mg II	2798	2014.6	10	39	16	60
		1980.7	8	33	8	31
[O II]	3726+29	2014.6	54	115	36	76
		1978.7	31	66	27	58
Hβ	4861	2014.6	26	35	24	33
		1978.7	17	23	22	30
[O III]	5007	2014.6	14	19	16	21
		1994.6	18	23	21	28
		1978.7	9	12	15	20
[O I]	6300	2014.6	40	42	43	45
		1978.7	34	36	41	43
Hα	6563		100	100	100	100
[S II]	6716+30	2014.6	87	85	46	45
		1994.6	68	66	40	41
		1978.7	49	48	38	37

where we have used equations (1-3) to write the shock luminosities in terms of the jet velocity v_j (second set of equalities) and in terms of the working surface velocity v_{ws} (third set of equalities). In these equations, $\dot{M}_j = \sigma\rho_j v_j$ is the total mass per unit time arriving at the working surface.

The total luminosity of the working surface then is:

$$L_{ws} = L_{js} + L_{bs} = \frac{\dot{M}_j}{2}\frac{(1-\alpha)^3}{(1+\alpha)^2}\left(\frac{v_{ws}}{\beta}\right)^2 . \quad (6)$$

As discussed in the previous section, the fact that the emission line ratios of HH 1 and 2 have changed very little implies that the shocks giving rise to the observed emission have relatively constant shock velocities. Unless one is prepared to believe in the presence of a calibrated balancing of different effects, the fact that we have constant jet shock or bow shock velocities (depending on which of the two shocks dominates the emission) implies constant values of v_j, $\beta = \sqrt{\rho_j/\rho_a}$ and $\alpha = v_a/v_j$ (see equations 2 and 3).

A less restrictive requirement is obtained for the regime of high β and low α. In this $\rho_j \gg \rho_a$ regime, the bow shock dominates the working surface luminosity (see equations 4-5), and $v_{ws} \approx v_j$ (see equation 1). Therefore, if any possible time-variability of the ejection of the jet manifests itself only over time periods longer than a few decades (which are covered by the observations), we would have an approximately constant $v_{bs} \approx v_{ws} \approx v_j$ (see equations 1 and 3), and the luminosity (dominated by the bow shock emission) would be given by equation (6) with constant v_{ws} (and $\alpha \ll 1$):

$$L_{ws} \approx \frac{\dot{M}_j}{2}\left(\frac{\rho_a}{\rho_j}\right)^2 v_{ws}^2 . \quad (7)$$

4.3. *Application of the working surface model to HH 1 and 2*

The emission line spectrum of HH 2, which shows basically time-independent line ratios (indicating a constant shock velocity) and a strongly increasing luminosity can then be directly interpreted as a jet (of constant velocity and mass loss rate) travelling in an environment of increasing density. From equation (7) we see that the increase in the environmental density is expected to be proportional to the observed increase in the luminosity.

For HH 1, we observe a small decrease in luminosity as a function of time (see Tables 1 and 2). In terms of our working surface model, this would then imply that HH 1 is moving into an ambient medium of slowly decreasing density (see equation 7).

Let us note that a "high β", "heavy jet" situation is consistent with the high proper motions observed in HH 1 and 2. These proper motions have remained almost constant from the mid-twentieth century (see Herbig & Jones 1981; Bally et al. 2002), implying that the presence of environmental inhomogeneities do not produce appreciable effects (as would be the case for a low β outflow, see equation 1). Interestingly, a small acceleration of the HH 1 proper motions has recently been measured (Raga et al. 2016), which would be consistent with a high β jet moving into a medium of decreasing density (see equation 1).

Implicit in this discussion is the expectation of a time-independent ratio between the luminosity of the lines we are studying (see Tables 1 and 2) and the continuum and line luminosities (at optical, UV and IR wavelengths) not considered in the present study. This appears to be a reasonable assumption given the fact that we are apparently having almost time-independent shock velocities in HH 1 and 2.

4.4. *The mass loss rate of the HH 1/2 system*

From Table 2, we see that the ratio of the luminosities of all of the lines (including Hα) we are considering to Hα lies in the range of 3 to 4 for HH 1 and 2. In the 1978.7 observations of Brugel et al. (1981a), one finds that the remaining lines (observed

by these authors, but not included in our present paper) contribute an extra $\approx 30\%$ to the luminosities of HH 1 and 2. The continuum of HH 1 and 2 has a luminosity of ≈ 2 times the Hα luminosity in the $\lambda = 3000$ to 8000 Å wavelength range (Brugel et al. 1981b).

The continuum in the $\lambda = 1300$ to 3000 Å wavelength range (Böhm-Vitense et al. 1982) has a luminosity of ≈ 15 times Hα. However, the reddening correction in the far UV is very uncertain (Böhm et al. 1991).

Considering the line and continuum contributions described above, we see that the total luminosity of HH 1 and 2 is at least ≈ 10 times the Hα luminosity. Therefore, in the first (1978.7) epoch, both HH 1 and HH 2 had total luminosities of $\approx 7 \times 10^{-2}\, L_\odot$ (see Table 1). Inserting this value in equation (7), we then obtain an estimate:

$$\dot{M}_j \approx 1.5 \times 10^{-8}\, M_\odot\, \mathrm{yr}^{-1} \times \left(\frac{L_{ws}}{7 \times 10^{-2} L_\odot}\right) \left(\frac{200\,\mathrm{km\,s^{-1}}}{v_{ws}}\right) \left(\frac{\rho_j}{\rho_a}\right)^2, \quad (8)$$

where we have used an estimate of 200 km s^{-1} for the velocity of HH 1 and 2 (see, e.g., Bally et al. 2002).

Since HH 1 and 2 appear to correspond to high β ($= \sqrt{\rho_j/\rho_a}$) working surfaces (see above), we would then conclude that the mass loss rate associated with each lobe of the outflow has a value $\dot{M}_j \approx 10^{-7} M_\odot \mathrm{yr}^{-1}$. This estimate of the mass loss rate lies within the range of mass loss rates deduced by Nisini et al. (2005) from observations of the optical and IR emission of the HH 1 jet.

5. CONCLUSIONS

A comparison of spectra of HH 1/2 obtained in three epochs, namely

1. 1978.7: spectrophotometric data of Brugel et al. (1981a),
2. 1994.6: 3 narrow-band HST images (Hester et al. 1998),
3. 2014.6: 7 narrow-band HST images (Raga et al. 2015a, b),

shows that the emission-line ratios do not change appreciably over this rather extended time period. This result is not completely surprising because the proper motion velocities of these objects have remained almost constant over a long time period (see Herbig & Jones 1981 and Bally et al. 2002).

More surprising is the fact that while the line intensities of HH 1 have remained almost constant (showing only a small decrease of $\approx 30\%$ in the 1978-2014 period), HH 2 has brightened by a remarkably large factor of ≈ 4. This scaling up of the brightness of HH 2 is unlikely to be the result of a change in the extinction to the object (as it travels away from the outflow source), because such a change would be directly visible as a time-dependence of the observed line ratios.

Therefore, we conclude that HH 2 appears to be moving into an ambient medium of increasing densities, while preserving the same shock velocity. This situation is consistent with the leading working surface of a "heavy" jet (i.e., with high $\beta = \sqrt{\rho_j/\rho_a}$, where ρ_j is the jet density and ρ_a the ambient density) moving into an inhomogeneous environment. Such a scenario is not unreasonable for the HH 1/2 system, which are located above the L1641 cloud, and with HH 2 (which is slightly redshifted) moving into a region in which denser condensations are present (see Girart et al. 2005; Lefloch et al. 2005).

A simple analytic model of a working surface shows that for a high β working surface the luminosity is proportional to ρ_a/ρ_j. Therefore, the increase of ≈ 4 in the brightness of HH 2 could be explained with a similar rise in the density of the environment into which HH 2 is travelling.

Of course, in this high β regime the changes in environmental density will also lead to (small) changes in the motion of the HH objects. The small decrease in the brightness of HH 1 (interpreted as the result of a decrease in the environmental density) would then be coupled with a small increase in the velocity of the object. It seems that such an effect is indeed observed (Raga et al. 2016).

Clearly, it will be necessary to carry out a new analysis of the proper motions of HH 2 (including the new HST images of Raga et al. 2015a, b) to see whether or not its increase in brightness is coupled with a small decrease in its proper motion velocities.

Another remaining point is that it is clear that the total (radiative) luminosity of an HH object provides a direct measure of the mechanical luminosity of the associated stellar outflow (see § 4.2). In § 4.4, we have used an estimate of the luminosities of HH 1 and 2 to obtain an estimate of the mass loss rate associated with this outflow. The luminosity that we have used is based on the optical line intensities (which have been measured at different epochs), the optical continuum (obtained only around 1980), and the line and continuum UV emission (also obtained around 1980). Notably, we did not include the IR

line and continuum emission (part ot this information is present in Spitzer and Herschel observations of the HH 1/2 region, see Noriega-Crespo & Raga 2012 and Fischer et al. 2010). A detailed analysis of current observations covering all of the relevant wavelength ranges would provide more reliable luminosities for HH 1 and 2, therefore leading to better estimates of the mass loss rate of the outflow.

Support for this work was provided by NASA through grant HST-GO-13484 from the Space Telescope Science Institute. AR acknowledges support from the CONACyT grants 167611 and 167625 and the DGAPA-UNAM grants IA103315, IA103115, IG100516 and IN109715.

REFERENCES

Bally, J., Heathcote, S., Reipurth, B., Morse, J., Hartigan, P., & Schwartz, R. 2002, AJ, 123, 2627
Böhm, K. H., Raga, A. C., Binette, L. 1991, PASP, 103, 85
Böhm, K. H., Noriega-Crespo, A., Solf, J. 1993, ApJ, 416, 647
Böhm-Vitense, E., Cardelli, J. A., Nemec, J. M., Böhm, K. H. 1982, ApJ, 262, 224
Brugel, E. W., Böhm, K. H., Mannery, E. 1981a, ApJS, 47, 117
_____. 1981b, ApJ, 243, 874
Brugel, E. W., Böhm, K. H., Böhm-Vitense, E., Shull, J. M. 1985, ApJ, 292, L75
Cardelli, J. A., Clayton, C. C., Mathis, J. S. 1988, ApJ, 239, L33
Eislöffel, J., Mundt, R., Böhm, K. H. 1994, AJ, 108, 1042
Fischer, W. J., Megeath, S. T., Ali, B. et al. 2010, A&A, 518, L122
Fitzpatrick, E. L. 1999, PASP, 111, 63
Giannini, T., Antoniucci, S., Nisini, B., Bacciotti, F., Podio, L. 2015, ApJ, 814, 52
Girart, J. M., Viti, S., Estalella, R., Williams, D. A. 2005, A&A, 439, 601
Hartigan, P., Raymond, J., Hartmann, L. W. 1987, ApJ, 316, 323
Hartigan, P. et al. 2011, ApJ, 736, 29
Herbig, G. H. 1969, CoKon, 65 (Vol VI, 1), 75
_____. 1973, IBVS, 832
Herbig, G. H., Jones, B. F. 1981, AJ, 86, 1232
Hester, J. J., Stapelfeldt, K. R., Scowen, P. A. 1998, AJ, 116, 372
Lefloch, B., Cernicharo, J., Cabrit, S., Cesarsky, D. 2005, A&A, 433, 217
Nisini, B., Bacciotti, F., Giannini, T.,Massi, F., Eislöffel, J., Podio, L., & Ray, T. P. 2005, A&A, 441, 159
Noriega-Crespo, A., Raga, A. C., 2012, ApJ, 750, 101
Oke, J. B. 1969, PASP, 81, 11
Raga, A. C., Barnes, P. J., Mateo, M. 1990a, AJ, 99, 1912
Raga, A. C., Cantó, L., Binette, L., Calvet, N. 1990b, ApJ, 364, 601
Raga, A. C., Reipurth, B., Castellanos-Ramírez, A., Chiang, Hsin-Fang, Bally, J. 2015a, AJ, 150, 105
_____. 2015b, ApJ, 798, L1
Raga, A. C., Reipurth, B., Esquivel, A., Bally, J. 2016, AJ, 151, 113
Raymond, J. C. 1979, ApJS, 39, 1
Schwartz, R. D., Cohen, M., Jones, B. F., Böhm, K. H. et al. 1993, AJ, 106, 740
Solf, J., Böhm, K. H., Raga, A. C. 1988, ApJ, 334, 229

J. Bally: Center for Astrophysics and Space Astronomy, University of Colorado, 389 UCB, Boulder, CO 80309-0389, USA.
A. C. Raga & A. Castellanos-Ramírez: Instituto de Ciencias Nucleares, Universidad Nacional Autónoma de México, Ap. 70-543, C.P. 04510, Ciudad de México, México (raga@nucleares.unam.mx).
B. Reipurth: Institute for Astronomy, University of Hawaii at Manoa, Hilo, HI 96720, USA.